Stir Zone Microstructure and Strain Rate during Al 7075-T6 Friction Stir Spot Welding

A. GERLICH, G. AVRAMOVIC-CINGARA, and T.H. NORTH

The factors determining the temperature, heating rate, microstructure, and strain rate in Al 7075-T6 friction stir spot welds are investigated. Stir zone microstructure was examined using a combination of transmission electron microscopy (TEM) and electron backscattered diffraction (EBSD) microscopy, while the strain rate during spot welding was calculated by incorporating measured temperatures and the average subgrain dimensions in the Zener–Hollomon relation. The highest temperature during friction stir spot welding (527 °C) was observed in spot welds made using a tool rotational speed of 3000 rpm. The stir zone regions comprised fine-grained, equiaxed, fully recrystallized microstructures. The calculated strain rate in Al 7075-T6 spot welds decreased from 650 to about 20 s^{-1} when the tool rotational speed increased from 1000 to 3000 rpm. It is suggested that the decrease in strain rate results when tool slippage occurs when the welding parameter settings facilitate transient local melting during the spot welding operation. Transient local melting and tool slippage are produced when the welding parameters produce sufficiently high heating rates and temperatures during spot welding. However, transient local melting and tool slippage is not produced in Al 7075-T6 spot welds made using a rotational speed of 1000 rpm since the peak temperature is always less than 475 °C.

I. INTRODUCTION

FRICTION stir welding was developed by TWI (Great Abington, Cambridge, U.K.) as an alternative to fusion welding for the fabrication of aluminum alloys.[1] The joining process has been used by the aerospace and automotive industries when joining a range of Al-alloy sheet materials such as Al 2024, Al 7075, Al 6111, and Al 5754. Although much research has been carried out when investigating the microstructures and mechanical properties of Al 7075-T6 friction stir welds produced using a wide range of processing conditions and tool geometries, the factors, which determine stir zone formation and microstructure, are not yet fully understood. Dynamic recrystallization has been cited to explain the formation of fine-grained equiaxed stir zone microstructures having grain sizes, which range from 1 to 10 μm.[2–5] Also, friction stir processing has been used to produce ultra-fine-grained material in bulk[6] and improve the mechanical properties of selected areas in components.[7]

Friction stir spot welding is a process variant of friction stir welding, where, instead of traversing the rotating tool across the workpiece, the welded joint is made by plunging the rotating tool into and out of overlapping Al-alloy sheets at a single location.[8,9] The power density during spot welding is considerable (around 10^{10} W/m^3),[10] the cycle time is very short (from 1 to 5 seconds), and the completed welds cool rapidly following completion of the welding operation. The influence of welding parameter settings on the microstructural features of the stir zones produced during Al 7075-T6 spot welding has not been investigated. With this in mind, the present article investigates the factors determining the microstructure, grain size, strain rate, and hardness of Al 7075-T6 welds produced using a range of tool rotational speeds.

Frigaard *et al.*[11] estimated the strain rate during friction stir spot welding of Al 6082 and Al 7108 sheet materials and reported values from 1.6 to 17 s^{-1}. These calculated strain rate values were an order of magnitude lower than those expected based on the tool rotational speed setting used during the friction stir welding operation. With this in mind, Frigaard *et al.*[11] suggested that the discrepancy was associated with local melting, which facilitated slippage between the tool periphery and adjacent material in the stir zone. The local melting proposal was underpinned by Droenen and Ryum's research,[12] which indicated that spontaneous melting of second-phase particles such as η and T phase occurred when Al-Zn-Mg test sections were rapidly upquenched. In subsequent research, Bjørneklett *et al.*[13] confirmed that, when samples of Al 7030 sheet were heated at 330 °C/s to the eutectic temperature (475 °C), 30 vol pct of the η particles were undissolved and melted spontaneously. In contrast, when a lower heating rate (100 °C/s) was applied, all η particles were dissolved when a temperature of 475 °C was reached. Based on these results, it was suggested that high heat inputs should be employed during friction stir welding to enable dissolution of second-phase particles prior to attainment of the eutectic temperature.

The present article investigates the factors determining the peak temperature and strain rate during Al 7075-T6 friction stir spot welding. It is well known that thermocouples embedded in Al-alloy sheet ahead of the traversing tool can be displaced by the dynamically recrystallized material, which is produced during the friction stir welding operation. This particular problem is avoided in the current study by embedding thermocouples within the tool itself, at the locations close to the tip of the rotating pin and midway between the pin periphery and the outer periphery of the tool shoulder. The strain rates in spot welds produced using a range of tool rotational speed settings are calculated by

A. GERLICH, Doctoral Student, G. AVRAMOVIC-CINGARA, Research Associate, and T.H. NORTH, Professor, are with the Department of Materials Science and Engineering, University of Toronto, Toronto, ON, Canada M5S 3E4. Contact e-mail: gerlich@ecf.utoronto.ca

Manuscript submitted January 17, 2006.

incorporating the measured temperature values and the average subgrain dimensions determined using transmission electron microscopy (TEM) in the Zener–Hollomon equation.

II. EXPERIMENTAL PROCEDURE

A. *Material*

The base material used was commercial 1.5-mm-thick Al 7075-T6 sheet having the chemical composition shown in Table I. The grains in the as-received sheet material were elongated, with an average diameter of 52 μm parallel to the rolling direction and 16 μm in the through-thickness direction.

B. *Processing*

The plunge rate (tool displacement rate) was 2.5 mm/s in all spot welding trials. The tool penetration depth was measured using a linear transducer having an accuracy of $\pm$0.01 mm, while the spindle rpm was measured using a shaft encoder, which had an accuracy of $\pm$30 rpm. The axial load and the torque values were measured using a six-axis load cell, which was coupled with a data acquisition system so that the axial force, torque, and penetration depth values were recorded simultaneously during each spot welding operation.

The target tool penetration depth was 2.2 mm during all spot welding trials and corresponded with the point when the tool shoulder just contacted the upper sheet surface. When the rotating pin was fully penetrated into the Al 7075-T6 sheets, the welding cycle was extended by incorporating a dwell time of up to 4 seconds. This facilitated investigation of the temperature changes when different dwell times were applied. The tool rotational speed remained constant while axial force and torque decreased during the dwell period. Due to machine compliance, the rotating tool penetrated 350 μm into the upper sheet during a 4-second dwell period. At the end of any selected dwell period, the rotating tool was retracted.

C. *Welding Parameter Selection*

All spot welding trials were carried out using an H13 (0.35 wt pct C, 5 wt pct Cr, 1.5 wt pct Mo, and 1 wt pct V) steel tool with a hardness of 46 to 48 HRC. The shoulder diameter was 10 mm, the pin diameter was 4 mm, and the pin length was 2.2 mm. The influence of tool rotational speed variations from 1000 to 3000 rpm was investigated in detail.

The energy resulting from tool rotation during friction stir spot welding is determined by the tool geometry (shoulder diameter, pin diameter, and pin length) and the welding parameter settings (tool rotational speed, plunge rate, and dwell time). However, the stir zone width is very narrow when tool rotational speed settings, $\leq$1000 rpm, are used without the application of a dwell time.[10] Consequently, the welding parameters selected in this investigation are those that produce stir zone widths $>$100 μm at the interface between the overlapping sheets and the resulting joints have bonded areas that are representative of typical spot welded joints.

Table I. Composition (Weight Percent)

Element	Zn	Mg	Cu	Cr	Mn	Si	Fe	Al
Al 7075-T6	5.41	2.34	1.27	0.21	$<$0.01	0.07	0.12	bal

D. *Testing and Characterization*

The thermal cycle during Al 7075-T6 spot welding was measured by embedding 0.25-mm diameter K-type thermocouples 0.2 mm from the tip of the rotating pin and 0.8 mm from the outer periphery of the tool shoulder (Figure 1). The thermocouples were inserted into 1.0-mm-diameter holes in the tool so that the thermocouple junction was in direct contact with dynamically recrystallized material produced during the spot welding operation. A 4-second dwell period was incorporated into the spot welding cycle when all temperature measurements were carried out. Temperature measurements were repeated at least three times at each welding parameter setting. The average temperature value is $\pm$6.4 °C of that indicated in any figure or table in spot welds produced using rotational speeds from 2000 to 3000 rpm. The amount of scatter was slightly higher in welding trials conducted using rotational speeds of 1000 and 1500 rpm. The reason for this increased scatter is unknown. The error bars shown on any graph indicate one standard deviation above and below the reported value.

The stir zone microstructures in air-cooled spot welds were compared with those in spot welds quenched in a mixture of methanol and liquid nitrogen at $-$80 °C within 1 second of weld termination. The cooling rates and average grain dimensions in air-cooled and quenched spot welds made using identical welding parameter settings were compared. The cooling rate was evaluated by drilling a 0.8-mm hole midway through the upper Al 7075-T6 sheet at the location 1.8 mm from the periphery of the tool shoulder. A 0.25-mm K-type thermocouple was embedded at this location and fixed in place using thermal transfer paste. Early in the friction stir spot welding operation, dynamically recrystallized aluminum is forced into the hole and secures the thermocouple in position.

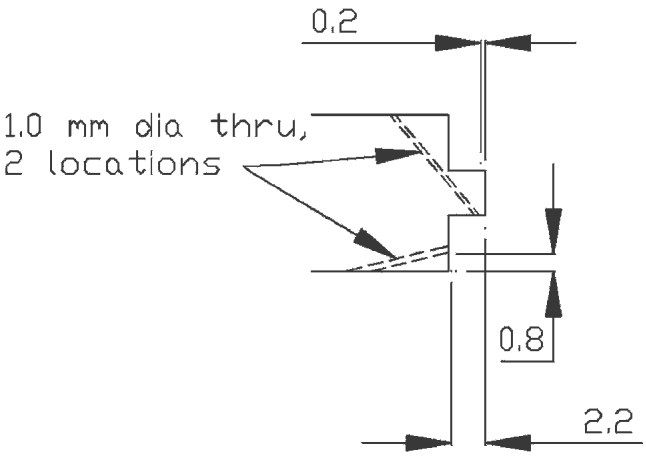

Fig. 1—Schematic showing the thermocouple locations in the friction stir spot welding tool (all dimensions are in millimeters).

All microhardness measurements were made using a Shimadzu (Kyoto, Japan) HMV-2 tester using a 0.49 N load and a holding time during testing of 10 seconds. Softening in the location beneath the base of the rotating pin was examined in spot welds made using different dwell times and tool rotational speeds. The welds were placed in liquid nitrogen immediately following the spot welding operation and were subsequently held in cold storage at a temperature of −20 °C to avoid natural aging of the welded samples at room temperature. The hardness of as-received and solution-treated Al 7075 sheet was measured. Some weld samples were solution treated at 465 °C for 2 hours. The microhardness of solution-treated spot weld samples was also evaluated following 7 days at room temperature.

All test sections examined using polarized light microscopy were anodized using 3 vol pct solution of HBF_4 at 30 V for 4 minutes. Transmission electron microscopy was performed on Hitachi H-800 and FEI-TECNAI 20 instruments (Tokyo, Japan) operating at 200 kV. All test specimens from the stir zone were obtained by sectioning the spot-welded joints using a Struers (Glasgow, U.K.) Accutom-2 low-speed saw, followed by grinding to a thickness of about 200 μm. The 3-mm disks were then thinned using a twin-jet electropolishing technique in a solution of 25 vol pct of HNO_3 and 75 vol pct of methanol at a temperature of –30 °C and a voltage of 12 V. The average grain dimensions in the stir zone were determined using planimetry by examining at least 50 grains on each TEM specimen. A minimum of two TEM samples were examined at each welding condition. The subgrain misorientation angle was measured by observing the angle of rotation of the selected area diffraction (SAD) pattern on crossing the boundary.

Electron backscattered diffraction (EBSD) was also used to obtain detailed quantitative information concerning the stir zone microstructure. All EBSD samples were sectioned parallel to the rolling direction in the Al 7075-T6 sheet and had the dimensions 80 μm in the radial direction and 15 μm in the tangential direction. The grain boundary statistics were determined using a Hitachi S-4500 field emission scanning electron microscope with TSL TexSEM software. Prior to EBSD, the surface of each sample was ground using 1200-grit SiC, and final electropolishing was carried out using similar preparation conditions to those during TEM microscopy. The step size was 0.25 μm during EBSD and the angular resolution limit of the equipment was around 2 deg. All misorientation output was processed using a ''clean-up'' algorithm, where individual points not belonging to a neighboring grain and points indexed with less than 1 pct confidence were interpolated to the average orientation of neighboring points.

III. RESULTS

A. *Temperature Measurement*

Figure 2 shows the axial force and temperature output produced during spot welding using a rotational speed of 2250 rpm. The axial force increases rapidly when the rotating pin contacts the upper surface of the Al 7075-T6 sheet, and an initial peak in axial force is apparent at 0.9 seconds. The axial force decreases and then increases again before reaching its peak value 1.3 seconds following process initiation. This point in the spot welding cycle coincides with contact between the tool shoulder and the upper surface of the Al 7075-T6 sheet. Comparable axial force and torque output with that shown in Figure 2 was found in spot welds made using rotational speed settings from 1000 to 3000 rpm. The reproducibility of the temperature output during Al 7075-T6 spot welding is illustrated in Figure 3.

Figures 4 and 5 show that higher heating rates and temperatures are produced when the tool rotational speed increases during Al 7075-T6 spot welding. The heating rates represent the average experimental values found during the tool penetration period in spot welding (from 0.3 to 1.3 seconds). Depending on the dwell time applied, the temperature exceeds the reported solidus (eutectic) temperature of Al 7075-T6 material (475 °C)[14] in spot welds made using rotational speeds from 1500 to 3000 rpm (Figure 5). The highest temperature during friction stir spot welding (527 °C) was observed in spot welds made using a tool rotational speed of 3000 rpm and a dwell time of 4 seconds.

The temperature profiles in air-cooled and in quenched Al 7075-T6 spot welds were recorded. In each case, the rotating tool was extracted 5.2 seconds after initiation of the spot welding operation, and the average cooling rates

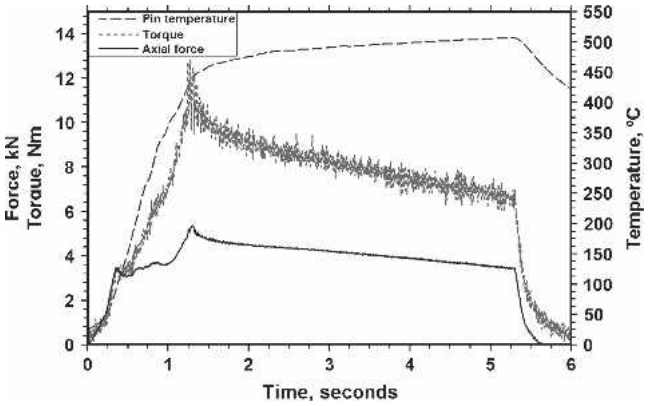

Fig. 2—Axial force and torque output and the measured temperatures in the location close to the tip of the rotating pin during Al 7075-T6 spot welding using a rotational speed of 2250 rpm.

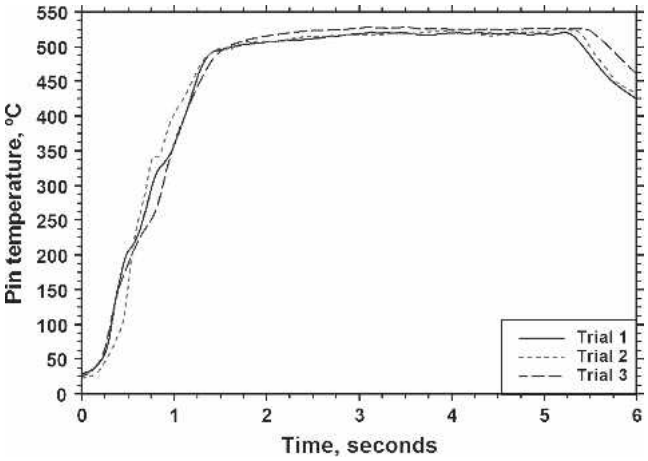

Fig. 3—Repeat tests showing the peak temperature output from the location close to the tip of the rotating pin during spot welding using a rotational speed of 3000 rpm and a dwell time of 4 seconds.

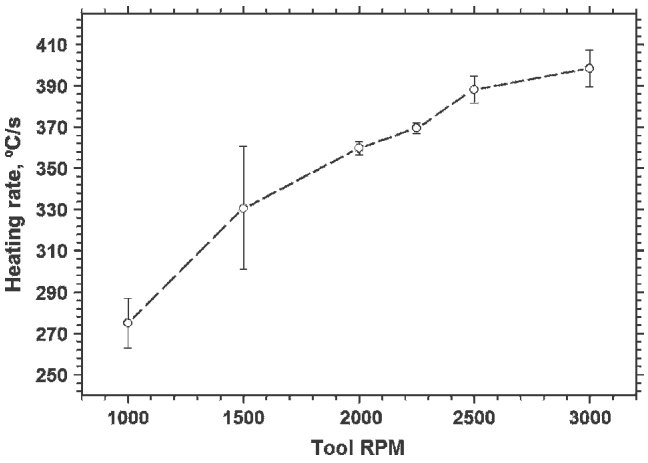

Fig. 4—The relation between tool rotational speed and the heating rate during the tool penetration stage in Al 7075-T6 spot welding. The error bars indicate standard deviations of heating rate values at any rotational speed setting.

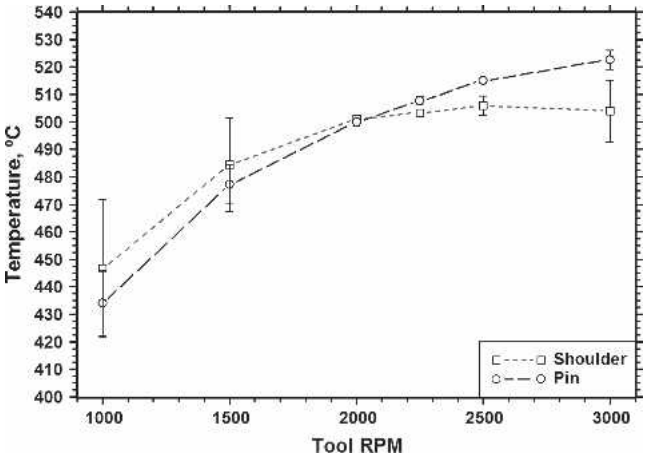

Fig. 5—Relation between tool rotational speed and temperature during spot welding using a dwell time of 4 s. The error bars indicate standard deviations of temperature values at any rotational speed setting.

following extraction were 120 °C/s in quenched spot welds and 40 °C/s in air-cooled spot welds.

B. *Spot Weld Hardness*

The optical microstructure shown in Figure 6 shows the transverse cross section of the weld zone and stir zone locations examined. Region I is in the stir zone region just above the sheet intersection, while region II is in the stir zone at the tool centerline immediately beneath the base of the keyhole. The hardness decreased to a minimum value at a distance of 2 to 3 mm from the keyhole periphery in a traverse across the stir zone region I and into the heat-affected zone region (Figure 7). The hardness approached that of as-received Al 7075-T6 sheet (178 HV) about 10 mm from the stir zone extremity. The repeatability of average hardness values was ±5 pct. The hardness values in the stir zone 7 days after the spot welding operation were similar to those in Al 7075 sheet, which was solution treated and aged at room temperature for 7 days (149 HV).

A number of Al 7075-T6 spot welds were quenched following tool extraction and were immersed in liquid nitrogen immediately following the spot welding operation. They were then held at −20 °C to prevent natural aging and reprecipitation. The hardness of the stir zone in the location immediately beneath the base of the keyhole decreased when higher tool rotational speeds and dwell time were applied (Figure 8). These results were found in spot welds, which were quenched and then cold stored prior to hardness measurement. The stir zone hardness was about 105 HV when dwell times exceeding 1 second were applied, regardless of tool rotational speed setting; this hardness value is similar to that of solution-treated Al 7075 sheet.

C. *Microstructural Features*

Figure 9 shows the microstructural features in the as-received Al 7075-T6 sheet material. The majority of particles in Figure 9 comprised either $Mg(Zn_2,AlCu)$ or $Mg_{32}(Al,Zn)_{49}$. The following intergranular particles were also confirmed: η' precipitates, Cr-based dispersoids, and η precipitates ($MgZn_2$). The grain boundary regions pinned by coarse Si-based and Fe-based particles could also be observed. The iron-based particles were either irregular in shape or were rodlike. Other particles detected at grain boundary regions comprised η, T phase ($Al_2Mg_3Zn_3$), and S phase (Al_2CuMg). These particles are typically found in Al 7075-T6 sheet material in the peak-aged condition.[2,13]

Both TEM and EBSD were used to determine the average grain sizes in the stir zone of spot welds made using different tool rotational speed settings. The average grain sizes in the stir zones of air-cooled and quenched spot welds were also determined. The stir zone widths in spot welds made using a tool rotational speed of 1000 rpm and dwell times of 0 and 1 seconds were too narrow for successful extraction of TEM specimens. However, in spot welds produced using this rotational speed setting and a dwell time of 4 seconds, the stir zone had a fine recrystallized grain structure (Figure 10). Also, when the tool rotational speed was increased to 3000 rpm, the stir zone microstructure in welds produced using a zero dwell time comprised recrystallized grains with an average diameter of 0.8 μm (Figure 11). However, strengthening η' precipitates were not detected in the stir zone (Figure 11(b)).

D. *Stir Zone Grain Size*

Table II shows that increasing the dwell time from 1 to 4 seconds had negligible influence on the stir zone crystallite dimensions in spot welds made using a rotational speed of 3000 rpm. The crystallite sizes determined using TEM in air-cooled and quenched welds ranged from 1.5 to 1.9 μm, confirming that grain growth did not occur when Al 7075-T6 spot welds cooled to room temperature following spot welding (Table II and Figure 12). The SAD results in Figure 12(c) show that the stir zone comprised crystallites, which were mostly separated by high-angle boundaries. However, some crystallites were detected which contained subgrains with low-angle boundaries.

Figure 13 shows the EBSD misorientation maps in the stir zone region 100 to 200 μm from the keyhole periphery (region I in Figure 6) in spot welds made using tool rotation speeds of 1500, 2250, and 3000 rpm. In Figure 13, subgrain boundaries having 2 to 15 deg misorientations

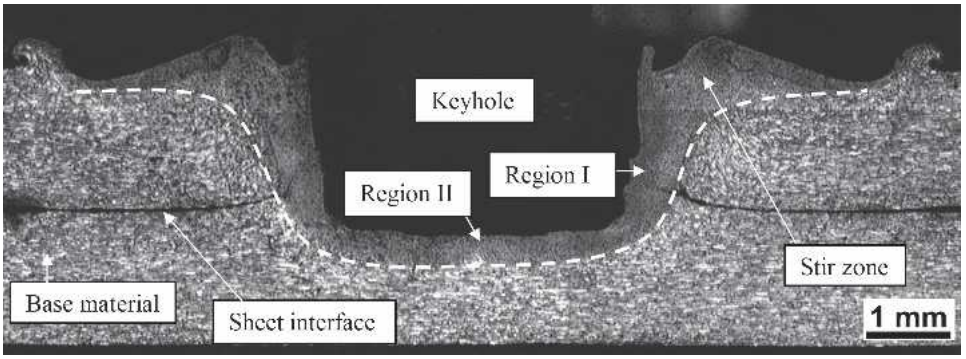

Fig. 6—Polarized light micrograph of a spot weld made using a rotational speed of 3000 rpm and a dwell time of 1 s. Boundary of stir zone is demarcated by a dashed line. Regions I (in the stir zone) and II (in the stir zone under the keyhole) show the locations examined using electron microscopy.

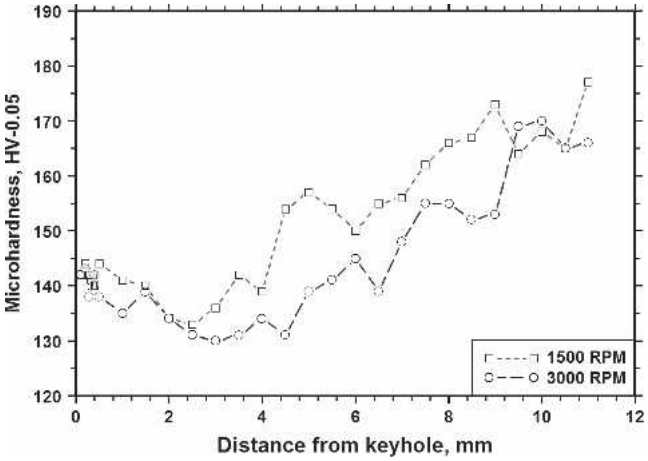

Fig. 7—Microhardness values adjacent to the keyhole through region I and horizontally across the weld shown in Fig. 2 for spot welds made using 1500 to 3000 rpm with 1-s dwell time.

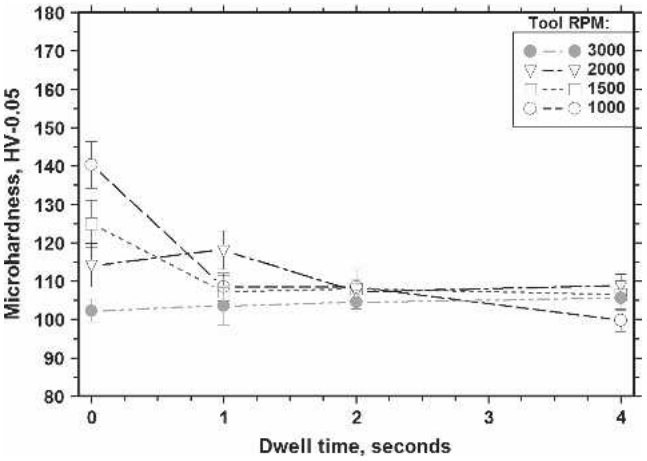

Fig. 8—Microhardness of the stir zone in quenched and cold-stored spot welds when using dwell times from 1 to 4 s and tool rotational speeds of 1000 to 3000 rpm. All samples were examined in the location immediately beneath the keyhole. The error bars indicate one standard deviation above and below the mean values.

are indicated by gray lines, while grain boundaries having >15 deg misorientations are indicated by black lines. The misorientation maps reveal that a fine, equiaxed grain structure comprising mainly high-angle grain boundaries exists in the stir zone. Similar misorientation maps were generated in spot welds produced using dwell times of 1 and 4 seconds. The fraction of high-angle grain boundaries having misorientations >15 deg varied from 58.9 to 74.8 pct in spot welds produced using different tool rotational speeds and dwell times (Table III). The high proportion of high-angle boundary regions and the fine-equiaxed grain sizes again suggests that the stir zone was mostly recrystallized.

Table IV shows the grain and subgrain dimensions in air-cooled Al 7075-T6 welds. The average EBSD grain dimensions were calculated from misorientation maps using the linear intercept method where only grain boundaries having >2 deg misorientations were considered. The average subgrain dimensions found using TEM were similar to those estimated using EBSD. Increasing the tool rotational speed had the largest influence on grain size.

E. *Estimated Strain Rate during Spot Welding*

The strain rate and temperature are related as follows during high-temperature deformation:

$$Z = \dot{\varepsilon} \exp\left(\frac{Q}{RT}\right) \quad [1]$$

where Z is the Zener–Hollomon parameter (the temperature-compensated strain rate), $\dot{\varepsilon}$ is the strain rate, T is the deformation temperature, Q is the activation energy, and R is the universal gas constant.[15] For a number of aluminum alloys, the Zener–Hollomon parameter and the subgrain diameter, d, are related as follows:[16–21]

$$d^{-1} = a + b \log(Z) \quad [2]$$

where a and b are constitutive constants. Equations [1] and [2] provide a ready means of estimating the strain rate during friction stir spot welding provided that accurate values for the subgrain dimensions and the deformation temperatures are available. However, it is apparent from Eqs. [1] and [2] that a small change in the average subgrain size will have a significant effect on the calculated strain rate. For example, the calculated strain rates at a temperature of 470 °C decrease from 67 to 3 s^{-1} when the subgrain size

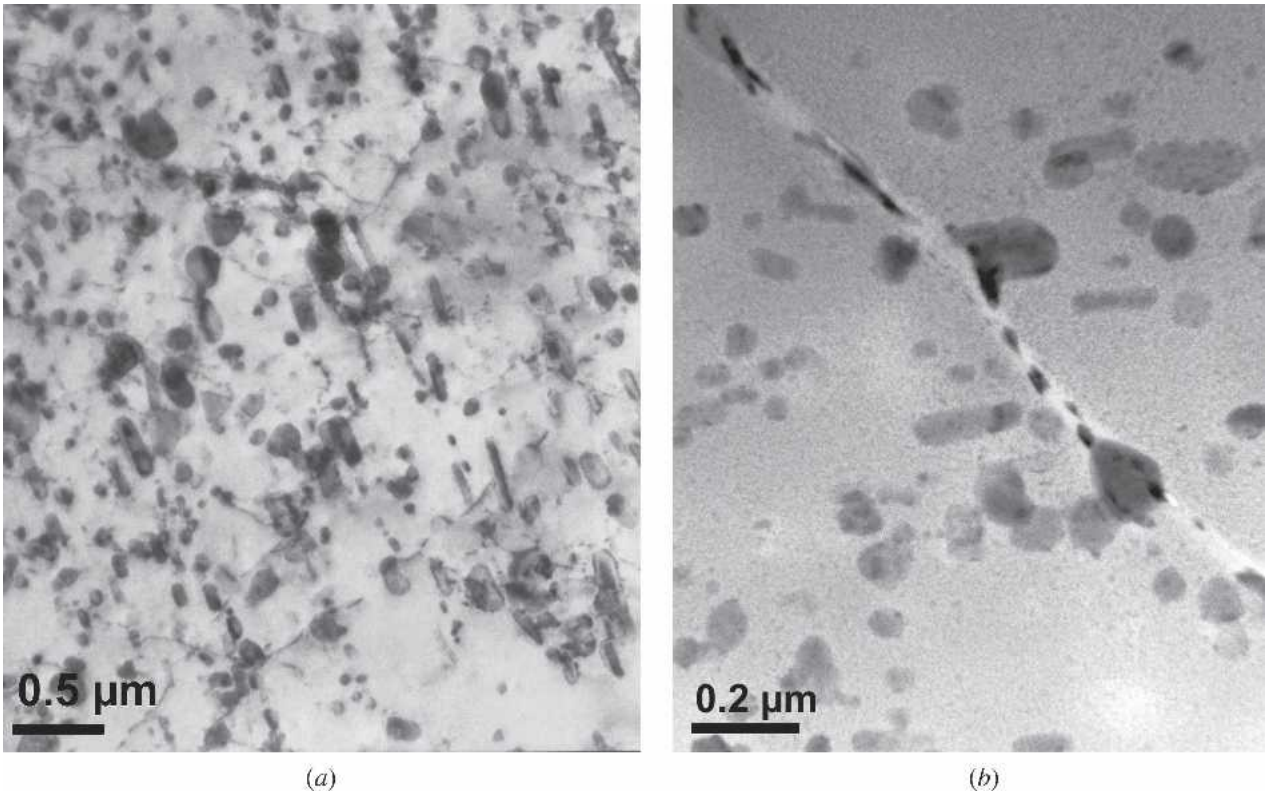

Fig. 9—TEM micrographs showing (*a*) $Mg(Zn_2,AlCu)$ and $Mg_{32}(Al,Zn)_{49}$, in the as-received Al 7075-T6 sheet, and (*b*) $MgZn_2$ particles at the grain boundary in the precipitation-free zone.

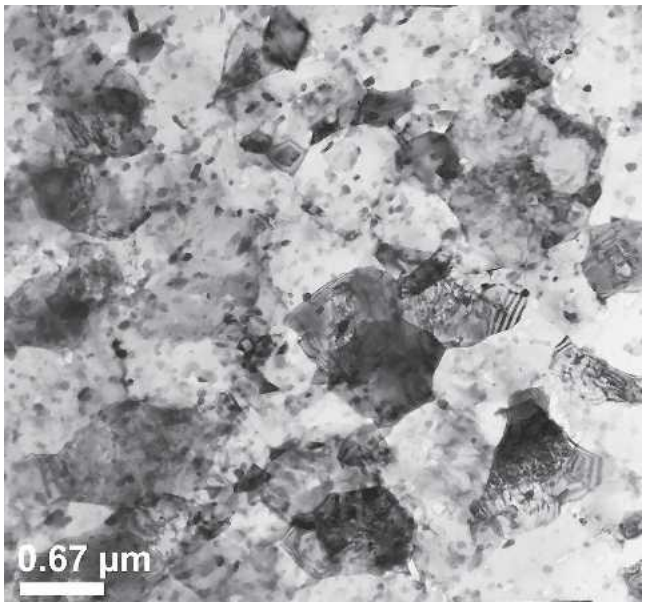

Fig. 10—Stir zone microstructure in a quenched spot weld made using a tool rotation speed of 1000 rpm and a dwell time of 4 s.

increases from 1.0 to 2.0 μm. For this reason, accurate measurements of the deformation temperature and subgrain size are required in order to obtain reasonable estimates of the strain rate during spot welding.

Table IV shows the average subgrain dimensions determined using TEM in the location 100 to 200 μm from the keyhole periphery in spot welds made using different tool rotational speeds and a dwell time of 4 seconds. The strain rate during spot welding was calculated in each case using the constants determined by Cerri *et al.*[20] for the Al 7075-T6 alloy sheet material, namely, $Q = 143$ kJ/mol, $a = 3.43$, and $b = 0.162$. In this connection, similar strain rate values were calculated using the constitutive constants developed by Sheppard for Al 7075-T6 sheet material.[21] Figure 14 shows the relation between the calculated strain rate and the rotational speed during Al 7075-T6 spot welding. The calculated strain rate decreased from 650 to about 20 s^{-1} when the tool rotational speed increased from 1000 to 3000 rpm. The calculated strain rates determined using average grain sizes found by EBSD produced similar values.

It is worth noting that the peak temperatures in Figure 5 and the calculated strain rates in Figure 14 are much higher than those generally applied during torsion testing experiments. For example, Hassan *et al.* used a test temperature of 470 °C and limited the strain rate to 0.005 s^{-1} during torsion testing in order to prevent specimen fracture during torsion testing of Al 7010 material.[22]

IV. DISCUSSION

A. *Particle Dissolution during Spot Welding*

In quenched spot welds made using a tool rotational speed of 1000 rpm and zero dwell time, recrystallized grains were not observed in the location immediately below the keyhole at the tool centerline. Selected area diffraction (SAD) patterns confirmed that η' particles were not

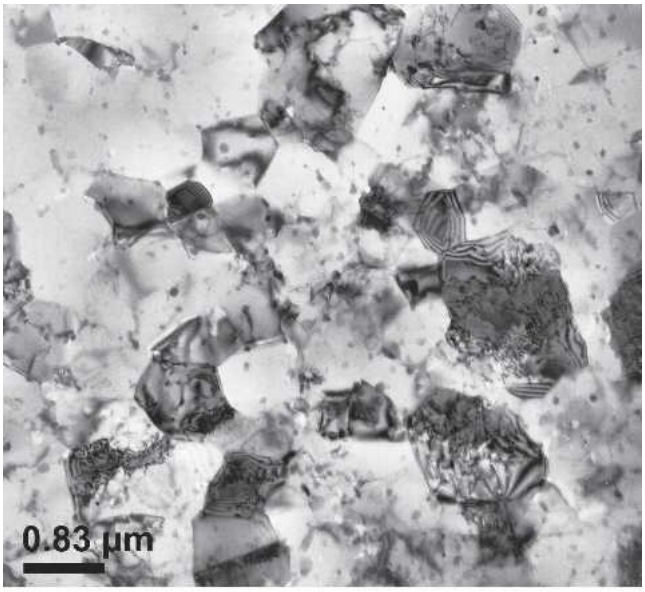

(*a*)

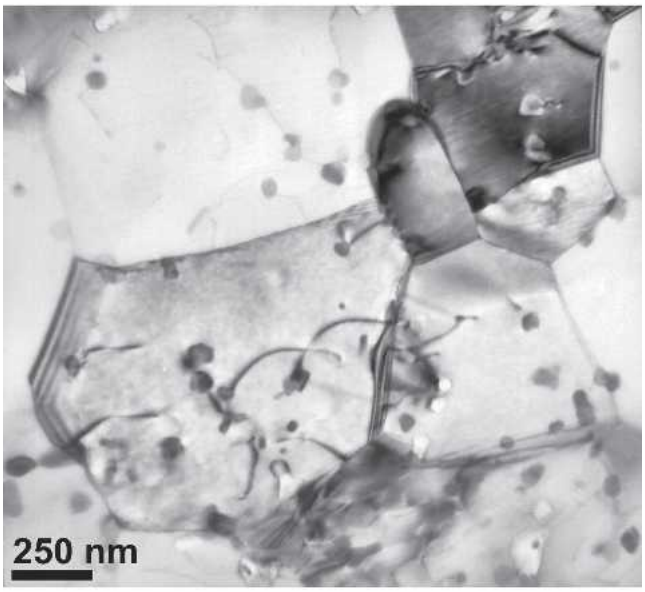

(*b*)

Fig. 11—Microstructure of the stir zone immediately beneath the keyhole in a spot weld produced using a rotational speed of 3000 rpm and zero dwell time. The spot weld was quenched following tool withdrawal: (*a*) small recrystallized grains having an average diameter of 0.8 μm and (*b*) particles within the stir zone.

dissolved and this particular spot weld had the highest hardness in the stir zone (Figure 8). However, recrystallized grains were observed in the stir zones of Al 7075-T6 spot welds made using a rotational speed of 3000 rpm and zero dwell time (Figure 11). The temperature attained when the rotating pin is fully penetrated (486 °C) in spot welds produced using a rotational speed of 3000 rpm is much higher than that required for dissolution of η' particles in Al 7050 and Al 7075 materials (180 °C to 260 °C).[23] Strengthening η' particles therefore were dissolved when the stir zone formed during spot welding. Dissolution and reprecipitation of η' particles during cooling to room temperature following the welding operation has already been reported in Al 7050 friction stir welds.[5]

The Cr-bearing, Fe-bearing, and $Al_6(Cu,Fe)$ dispersoids were identified in the stir zones of spot welds made using a rotational speed of 3000 rpm and dwell times of 1 and 4 seconds (Figures 15(a) and (b)). There was no influence of dwell time on the particle dimensions or particle distributions. Since almost all of the second-phase particles had similar dimensions (80 to 100 nm), it is possible that thermomechanical processing during stir zone formation may have facilitated particle fracture, as has been suggested previously when investigating friction stir seam welds.[5] Figure 15(b) shows that small numbers of coarse SiO_2 particles having dimensions similar to those of crystallites (about 1.7 μm) were also present in the stir zone. Both EDX and SAD also confirmed the presence of small contents of S phase.

B. *Stir Zone Grain Size*

The original microstructure in the as-received Al 7075-T6 sheet grain structure was completely replaced by fine-equiaxed grains in the stir zone. Some grains were formed individually and had high-angle boundaries, while others comprised two or more subgrains. The average crystallite dimensions were unchanged when the dwell time increased from 1 to 4 seconds in spot welds made using a rotational speed of 3000 rpm (Table IV). However, the grain diameter increased from 0.8 to 1.8 μm when the dwell time increased in spot welds made using a rotational speed of 1500 rpm.

The average grain size in the stir zone increased when higher tool rotational speed settings were employed (Table IV). Similar relations between stir zone grain size and tool rotational speed have been reported in Al-alloy and Mg-alloy friction stir welds.[24–27] Increasing the tool rotational speed from 1000 to 3000 rpm also increased the peak temperature during Al 7075-T6 spot welding (Figure 5). Sato *et al.*[24] noted a similar relation between tool rotational speed and temperature during friction stir welding of Al 6063 sheet and suggested that grain growth occurred when the welded joints cooled to room temperature. However, Table II shows that there was no evidence of grain growth during cooling of Al 7075-T6 spot welds. In this connection, Gerlich *et al.*[28] also found no evidence of grain growth when Al 5754 friction stir spot welds cooled to room temperature.

Both EBSD and TEM microscopy produced similar average crystallite dimensions in the stir zones of Al 7075-T6 spot welds (Table IV and Figure 13). While TEM microscopy and EBSD are capable of resolving individual grains, which have similar dimensions and morphologies, TEM is able to distinguish crystallites, which have much smaller misorientations (<2 deg). During EBSD, subgrain boundaries having misorientations <2 deg and dimensions <0.5 μm were not taken into account when the average grain dimensions were estimated, since step size was 0.5 μm and the available equipment had an angular resolution limit of 2 deg. However, Humphreys has pointed out that EBSD produces average grain size values, which are within 10 pct of those found using TEM provided that at least 5 pixels per grain are captured.[29] In this manner, sufficient numbers of pixels are

Table II. Crystallite Dimensions in Spot Welds Made Using a Rotational Speed of 3000 rpm (Measured Using TEM)

Parameter	1-s Welding Time				4-s Welding Time			
Postweld	Air-cooled		Quenched		Air-cooled		Quenched	
Location	stir zone*	under the keyhole**	stir zone	under the keyhole	stir zone	under the keyhole	stir zone	under the keyhole
Diameter, d_{av}	1.6 μm	1.8 μm	1.5 μm	1.9 μm	1.7 μm	1.7 μm	1.6 μm	1.8 μm

*Specimens extracted from region I in Fig. 6.
**Specimens extracted from region II in Fig. 6.

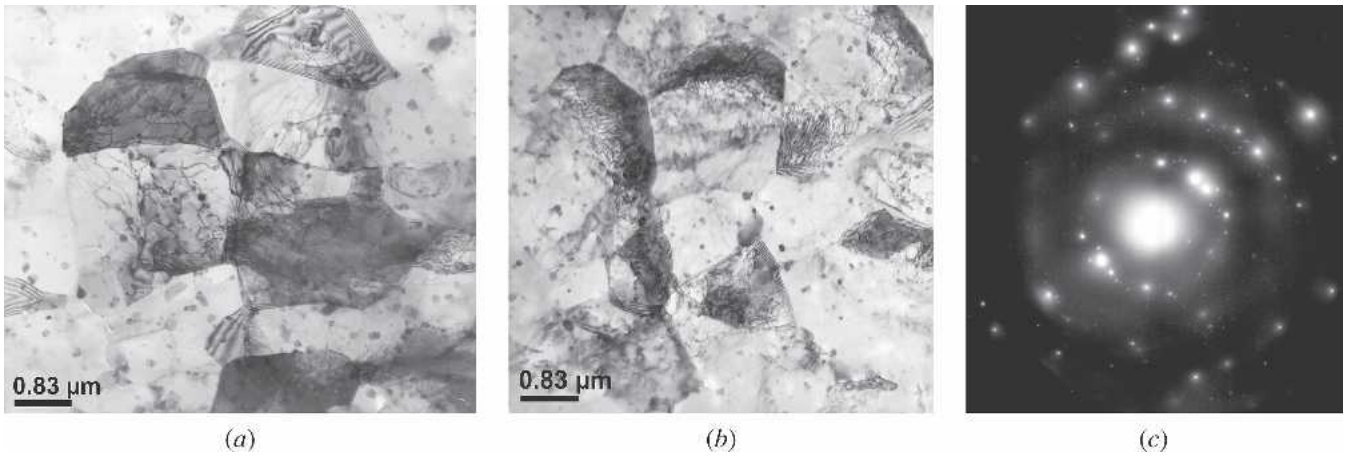

Fig. 12—Microstructure of the stir zone produced using a rotational speed of 3000 rpm and a dwell time of 4 s: (*a*) air-cooled spot weld and (*b*) quenched spot weld. (*c*) Typical diffraction pattern showing a mixture of low- and high-angle boundaries.

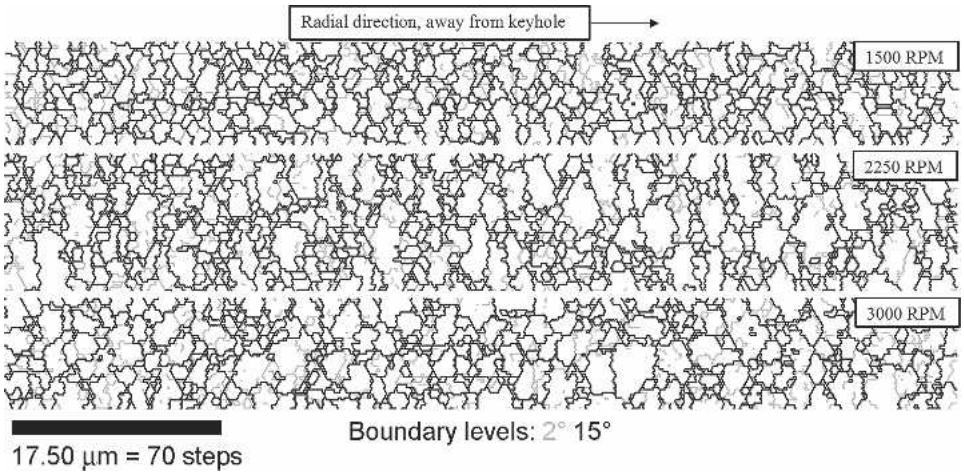

Fig. 13—EBSD misorientation maps showing subgrain boundaries (gray lines) and grain boundaries (black thick lines). The grain structures in the stir zones of spot welds produced using tool rotational speeds of 1500, 2250, and 3000 rpm and a dwell time of 1 s.

captured to reconstruct each grain in the misorientation map. Since the 0.25-μm step size used in the current study corresponds with an average of 17 to 25 pixels per grain, it is not surprising that the average crystallite dimensions found using EBSD and TEM are similar.

In Al 7075-T6 stir zones, about 65 pct of the grain boundaries had misorientations >15 deg, which is consistent with fully recrystallized microstructures (Table III). In a similar manner, Karlsen *et al.* noted that 87.5 pct of the grains in the stir zones of Al 7075 friction stir welds had high-angle boundaries.[30] Finally, there was no evidence of formation of the ''onion ring'' structures observed in the nugget regions of friction stir welds,[31] since no lateral movement of the rotating tool occurred during the spot welding operation.

C. *Calculated Strain Rates*

Frost and Ashby[32] have indicated that the Zener–Hollomon relation is most suited to describing deformation at high temperature and high strain rates. Also, different investigators have argued that the microstructural features

Table III. Misorientation Statistics Determined Using EBSD

Rotation Speed	1500 rpm		2250 rpm		3000 rpm	
Dwell Time	1 s	4 s	1 s	4 s	1 s	4 s
1 to 5 deg	32.8 pct	22.1 pct	36.5 pct	34.8 pct	27.0 pct	28.6 pct
5 to 15 deg	3.5 pct	3.1 pct	4.6 pct	3.0 pct	6.3 pct	7.8 pct
>15 deg	63.7 pct	74.8 pct	58.9 pct	62.3 pct	66.7 pct	62.6 pct

Table IV. Average Grain (Subgrain) Dimensions in Air-Cooled Al 7075-T6 Spot Welds

	TEM Subgrain Diameter (μm)		EBSD Grain Diameter (μm)	
Tool rpm	1-s weld	4-s weld	1-s weld	4-s weld
1000	—	0.64 ± 0.08	—	—
1500	0.80 ± 0.10	1.29 ± 0.14	0.95 ± 0.09	0.95 ± 0.10
2250	1.49 ± 0.09	1.73 ± 0.15	1.13 ± 0.19	1.08 ± 0.05
3000	1.53 ± 0.08	1.69 ± 0.12	1.85 ± 0.15	1.86 ± 0.16

*All TEM and EBSD output was obtained from region I in Fig. 6. The ranges indicate one standard deviation when examining test specimens using TEM or particular test samples when using EBSD.

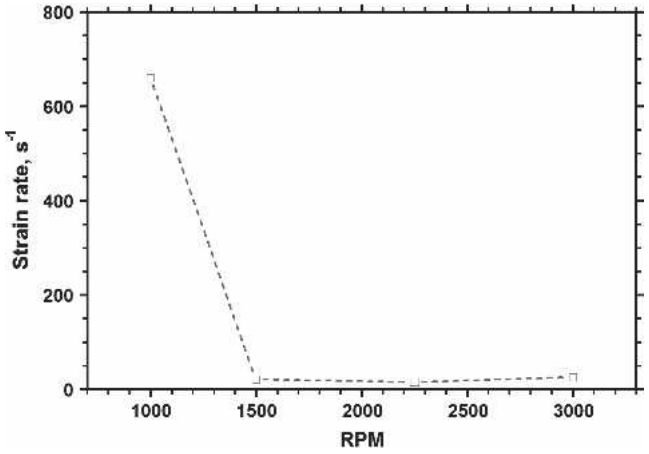

Fig. 14—Calculated strain rate values in Al 7075-T6 spot welds made using different rotational speed settings. The dwell time was 4 s and the plunge rate was 2.5 mm/s in all cases.

in friction stir welds can be readily examined using the Zener–Hollomon relation.[11,22,25,33] It has also been suggested that the Zener–Hollomon parameter calculated during numerical modeling can be used to predict the grain size and microstructure in the stir zone of friction stir welds.[34]

Reliable strain rate values can be estimated using the Zener–Hollomon relation provided that the peak temperate and average grain in a specific location can be accurately determined. As mentioned earlier, it is difficult to obtain consistent temperature output when thermocouples are embedded in the Al-alloy sheet ahead of the traversing tool during friction stir welding of long seams, since dynamically recrystallized material displaces thermocouples from their original locations.[35] Also, a steep temperature gradient exists adjacent to the tool periphery and the temperature decreases markedly at small distances from the contact surface.[35–39] This is precisely why investigators such as Bowden[36,37] and Quinn[39] used extremely sophisticated measuring techniques when measuring the peak temperatures resulting from frictional heating at contacting interfaces.

Figure 14 shows the relation between the calculated strain rate and the tool rotational speed in Al 7075-T6 spot welds produced using a dwell time of 4 seconds. The calculated strain rate decreased from 650 to about 20 seconds^{-1} when the tool rotational speed increased from 1000 to 3000 rpm. Also, a change in tool rotational speed from 1500 to 3000 rpm had negligible influence on the calculated strain rate.

If it is assumed that a no-slip condition exists at the contact interface and the shear strain rate decreases linearly when spot welding using a 4-mm-diameter rotating pin and a rotational speed of 3000 rpm, the strain rate midway across a 600-μm-wide stir zone should be around 1050 s^{-1}. Calculated strain rate values around 20 s^{-1} in Figure 14 therefore are remarkably low and are of the same order as those found during friction stir welding of Al 7030 (from 1.6 to 17.3 seconds^{-1}).[11] Frigaard *et al.*[11] suggested that the difference between the expected and actual calculated strain rate values resulted from local melting and tool slippage at the contact interface between the rotating tool and adjacent material in the stir zone.

D. *Local Melting during Al 7075 Spot Welding*

Bendzsak[35] and North[40] proposed that the peak temperature during friction stir welding of Al-alloy sheet material will fluctuate above and below the solidus temperature based on the following argument. Viscous dissipation of mechanical energy raises the temperature of the stir zone to the solidus temperature and local melting occurs when this temperature is exceeded. The viscosity of material immediately adjacent to the contact interface suddenly decreases and the heating rate and temperature decrease so that local melted films solidify. The material viscosity and the rate of heat generation both increase again, the solidus temperature is

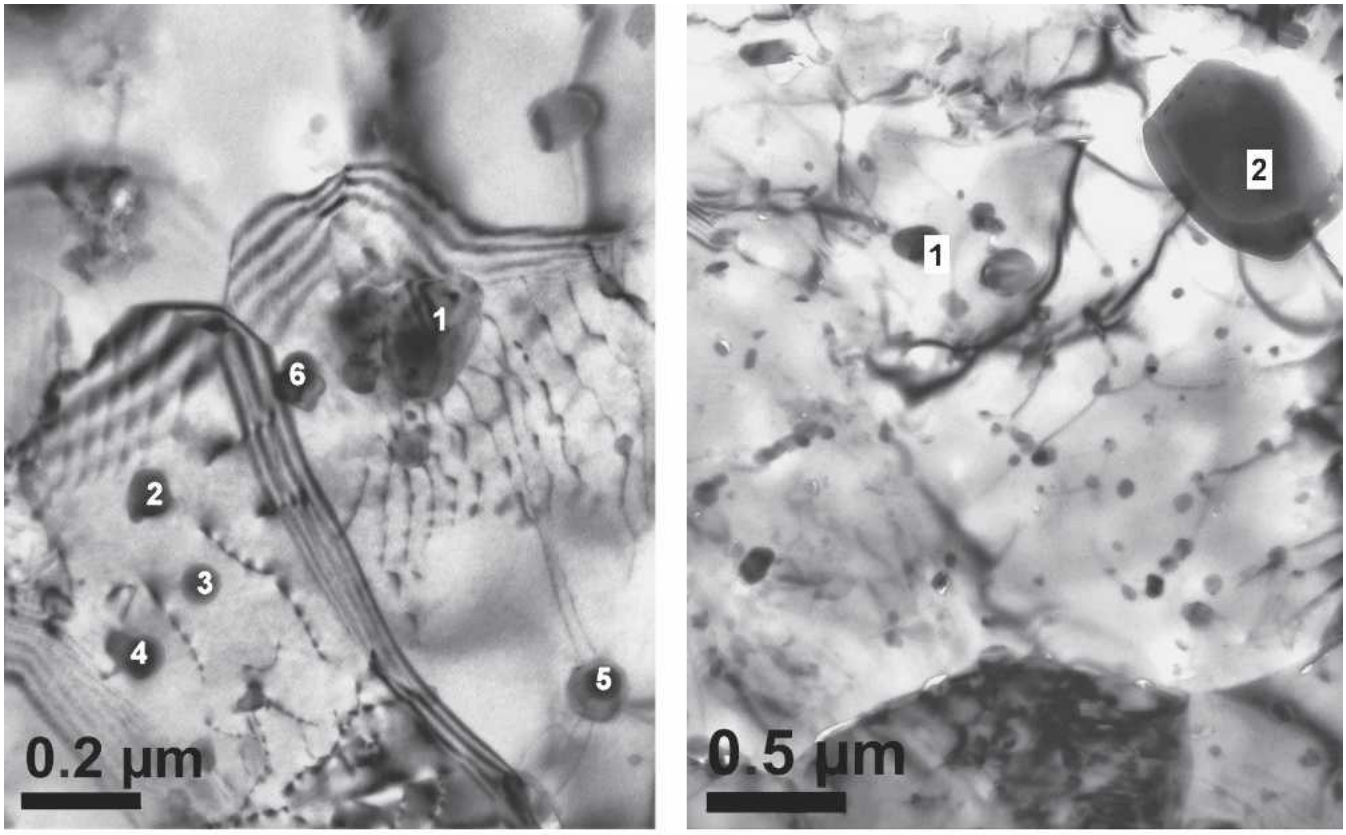

Fig. 15—TEM micrographs of the stir zone in a quenched spot weld made using a rotational speed of 3000 rpm and a dwell time of 4 s. The second-phase particles were characterized using EDX: (*a*) 1, 2, 4, 5, and 6 Cr bearing dispersoids, (b) 1—Al_6(Cu,Fe), and 2—SiO_2.

again exceeded, and the local melted films reform. This transient local melting proposal has been used to explain why the peak temperatures in Al 5754, Al 6061, Al 6111, Al 7075, Al 2024, AZ91, AZ31, and AM60 spot welds closely correspond with their solidus temperatures.[38,41–44]

Local melting at grain boundary regions has been reported in Al 7010 friction stir seam welds.[45] It was argued that, upon cooling, a low-temperature liquid $\rightarrow$ α-Al + S + η ternary eutectic reaction resulted in elevated levels of Cu along grain boundaries. Also, Bjørneklett *et al.*[13] found metallographic evidence of local melting at grain boundary regions when samples of Al 7030 sheet were heated at 330 °C/s to the eutectic temperature (475 °C) and associated local melting with spontaneous melting of undissolved second-phase particles in the as-received Al 7030 base material. This heating rate is remarkably similar to that found during Al 7075-T6 friction stir spot welding (Figure 4). Yan *et al.*[46] also found metallographic evidence of local melting when welding Al 2024/SiC composite material and associated its formation with segregation of Cu and Mg at the SiC particle/matrix interface. Metallographic evidence of local melted film formation has also been reported in Al 2024-T3 friction stir seam welds,[47] in Al 6061-T6 Al_2O_3 plunge tests,[41] in AZ31 friction stir spot welds,[48] and in dissimilar Al 6111/AZ91 and dissimilar 1050/AZ31 friction stir welds.[42,49] Finally, Colegrove *et al.*[50] provided indirect evidence for local melting during Al 7075-T6 friction stir seam welding, by showing that a numerical model based on FLUENT* significantly over-estimated the power input during seam welding when a noslip condition was assumed at the contact interface. As a result, different tool geometries could not be discriminated in terms of their measured forces and torque values.

*FLUENT is a trademark of FLUENT Inc., Lebanon, NH.

A detailed examination of phases located at grain boundary regions in Al 7075 spot welds did not show conclusive evidence of increased Cu content similar to that found by Hassan *et al.*[45] However, it is possible that a liquid α-Al + S + η ternary eutectic formed at grain boundary regions and the voids shown in Figure 16 are the result of preferential attack during the electropolishing stage in TEM foil preparation. In this connection, it is worth noting that Su *et al.*[5] also showed grain boundary regions in Al 7050 friction stir seam welds, which contained numerous voids.

During spot welding, the likelihood of transient local melting and tool slippage at the contact interface between the rotating pin and adjacent material in the stir zone will be determined by the welding parameter settings, the temperature attained during welding, and the local melting tendency of second-phase particles in the Al-alloy sheet material. The temperature attained during spot welding will depend on the rotational speed setting (on the heating rate, Figure 4) and on the length of the dwell period. For example, the heating rate is 400 °C/s and the peak temperature

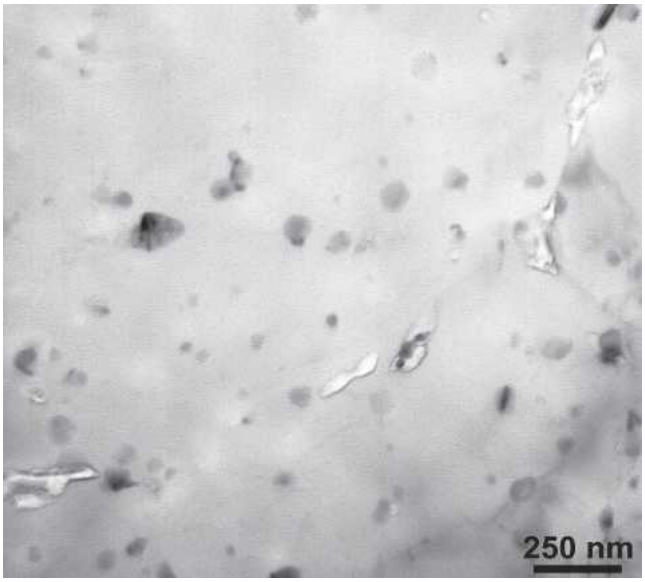

Fig. 16—TEM micrograph of voids preferentially occurring along grain boundaries in a quenched spot weld made using rotational speed of 3000 rpm and a dwell time of 1 s.

when the rotating pin is fully penetrated is 486 °C in spot welds made using a rotational speed of 3000 rpm. The temperature then increases to 527 °C during the dwell period and is close to the reported solidus temperature (532 °C) of well-homogenized Al 7075 material.[14]

The heating rates and temperatures attained during spot welding using different tool rotational speed settings and dwell times are indicated as follows.

The solidus temperature of Al 7075-T6 (475 °C) is only exceeded at the end of the 4-second-long dwell period in spot welds produced using a tool rotational speed of 1500 rpm. In contrast, the solidus temperature Al 7075-T6 is never reached in spot welds made using a rotational speed of 1000 rpm, no matter the dwell time that is applied (Table V).

The local melting tendency of second-phase particles will be determined by their constitution, dimensions, and distribution and in turn by the chemical composition and thermal history of the as-received Al-alloy sheet.[13] It is well documented that rapid upquenching of eutectic alloys such as Al-Mg-Zn, Al-Mg-Si, Al-Si, and Al-Cu facilitates spontaneous melting of second-phase particles, because they are not dissolved when the eutectic temperature is reached.[12,13,51–53] Figure 9 shows that grain boundary regions in the as-received Al 7075-T6 sheet were decorated with 120-nm-long and 50-nm-wide η particles. Since the heating rate varies from 270 °C/s to 400 °C/s depending on the tool rotational speed setting, it would be expected that spontaneous melting of undissolved η particles will occur when the peak temperature during Al 7075-T6 spot welding exceeds 475 °C.[13] Also, unmelted *T* and *S* phases located at grain boundary regions will melt spontaneously when the temperature during spot welding reaches 480 °C,[54] 489 °C,[12] and 490 °C.[54]

Table V shows that the temperature increases from 486 °C to 527 °C during the 4-second-long dwell period in spot welds made using a rotational speed of 3000 rpm. This increase in temperature during the dwell period in spot welding can be explained as follows. Rapid dissolution of spontaneously melted η particles and *S* and *T* phases will be facilitated by the high diffusion coefficient values of solute elements such as Mg and Zn at temperatures very close to the solidus temperature.[55] The kinetics of dissolution of spherical and platelike liquid drops close to the eutectic temperature during processing of Al-Cu alloy material has been examined by Reiso *et al.*[51] and Whelan.[56] Using their approach, the times required for dissolution of spherical and platelike liquid drops resulting from spontaneous melting at a temperature of 475 °C range from 0.06 to 3.0 seconds (Appendix).

When spontaneous melting occurs during spot welding, the material viscosity and the heating rate will suddenly decrease and the temperature will fall. The liquid films will solidify and the material viscosity and temperature will rise again. Continued repetition of this process will produce fluctuating peak temperature output during the dwell period in Al 7075-T6 spot welding. Figure 17 shows evidence of temperature fluctuations during the dwell period in spot welds made using rotational speeds of 2500 and 3000 rpm. However, it is important to note that corresponding torque fluctuations were not observed. It has been shown elsewhere that the torque measurement setup is not sensitive enough to detect the torque changes, which correspond with temperature changes of the order of 2 °C to 3 °C.[57] Only changes in temperature in the range from 8 °C to 14 °C produced observable fluctuations in torque output. Also, there was no evidence of temperature fluctuations during the dwell period in Al 7075-T6 spot welds made using tool rotational speeds of 1000 and 1500 rpm. The temperature only reached 477 °C at the end of the 4-second-long dwell period in spot welds produced using a rotational speed of 1500 rpm. In spot welds made using a rotational speed of 1000 rpm, the solidus temperature of Al 7075-T6 (475 °C) is never exceeded, no matter the dwell time that is applied (Table V).

It follows from the preceding discussion that tool slippage can occur at the contact interface between the tool periphery and adjacent material in the stir zone provided that the welding parameter settings facilitate transient local melting during the spot welding operation. When the cycle time, tool rotational speed, and dwell time produce temperatures $\geq$475 °C, this will facilitate transient local melting in the stir zone of Al 7075 welds and the strain rate during spot welding will be low because of tool slippage at the contact interface. This occurs in spot welds produced using rotational speed settings from 1500 to 3000 rpm. However, the peak temperature never reaches 475 °C and transient local melting and tool slippage does not occur in Al 7075-T6 spot welds made using a rotational speed of 1000 rpm, no matter the dwell time that is applied. It is worth noting that, although the results in the present article suggest that it might be possible to find particular welding parameter settings, which may prevent tool slippage during Al 7075-T6 spot welding, the width and volume of stir zone will be extremely small since the amount of energy generated during the spot welding operation is very limited.[10]

V. CONCLUSIONS

The factors determining the temperature, heating rate, microstructure, and strain rate in Al 7075-T6 friction stir

Table V. Influence of Rotational Speed on Heating Rate and the Peak Temperature during Al 7075-T6 Spot Welding Using Different Dwell Times

Rotational Speed (rpm)	Heating Rate (°C/s)	P.P.* (°C)	1-s Dwell (°C)	2-s Dwell (°C)	4-s Dwell (°C)
1000	275	340	380	406	434
1500	330	393	446	461	**477**
2000	360	424	472	**487**	500
2250	370	432	**483**	495	508
2500	388	455	**494**	505	515
3000	400	**486**	512	520	526

*P.P. is the point when the shoulder makes contact with upper sheet and dwell period begins.
Values in bold have been highlighted when temperature has first exceeded the solidus.

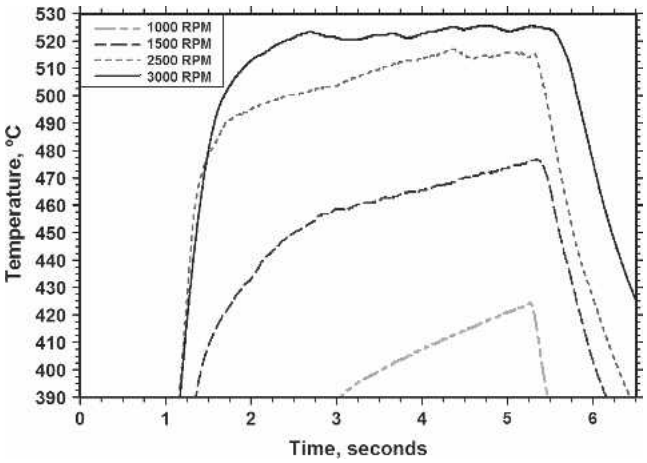

Fig. 17—Fluctuations in the peak temperature output during spot welding using rotational speeds from 2500 and 3000 rpm and 4-s dwell time. Temperature outputs without fluctuations using 1000 and 1500 rpm are included for comparison purposes.

spot welds produced using different tool rotational speed settings were investigated. Stir zone microstructure was examined using a combination of TEM and EBSD microscopy, while the strain rate during spot welding was calculated by incorporating measured temperatures and the average subgrain dimensions determined using TEM in the Zener–Hollomon equation. The following conclusions can be drawn from this research.

1. During spot welding the original microstructure in the as-received Al 7075-T6 sheet was completely replaced by a fine-grained, equiaxed, fully recrystallized microstructure in the stir zone. The EBSD confirmed that round 65 pct of the grain boundary regions in the stir zone had misorientations >15 deg. The average crystallite dimensions within the stir zone were negligibly affected when the dwell time increased from 1 to 4 seconds; there was also no evidence of grain growth when Al 7075-T6 spot welds cooled to room temperature.
2. The temperature exceeds the reported solidus temperature of Al 7075-T6 material (475 °C) in spot welds made using tool rotational speeds from 1500 to 3000 rpm. The highest temperature during friction stir spot welding (527 °C) was observed in spot welds made using a tool rotational speed of 3000 rpm and a dwell time of 4 seconds. However, the peak temperature never reached 475 °C in Al 7075-T6 spot welds made using a rotational speed of 1000 rpm no matter the dwell time that was applied.
3. The calculated strain rate during spot welding decreased from 650 to about 20 s^{-1} when the tool rotational speed increased from 1000 to 3000 rpm. It is suggested that this remarkable change in strain rate values when the tool rotational speed increases is associated with local melting and tool slippage, which occurs when the welding parameter settings facilitate transient local melting during Al 7075-T6 spot welding. Transient local melting and tool slippage occur at the contact interface between the periphery of the rotating tool and adjacent material in the stir zone when the cycle time, tool rotational speed, and dwell time produce high heating rates and temperatures during the spot welding operation. In contrast, transient local melting and tool slippage does not occur no matter the dwell time, which is applied when Al 7075-T6 sheet is spot welded using a rotational speed of 1000 rpm.

APPENDIX

Assuming that the liquid drops have a spherical geometry, the radius R will decrease with holding time according to the relation

$$\left(\frac{R}{R_0}\right)^2 = 1 - t\left(\frac{a}{R_o}\right)^2$$

where R_0 is the initial radius, t is time, and a is a constant, which depends on the driving force for solute diffusion. Following the methodology developed by Reiso *et al.,* when they examined dissolution of liquid drops in Al-Cu material,[51]

$$a^2 = 2D\left[\frac{C_{T_2}^{\alpha/\mathrm{liq}} - C_{T_1}^{\alpha/\beta}}{C_{T_2}^{\mathrm{liq}/\alpha} - C_{T_2}^{\alpha/\mathrm{liq}}}\right]$$

where $C_{T_2}^{\alpha/\mathrm{liq}} = 17\%$ is the solubility limit of $MgZn_2$, $C_{T_1}^{\alpha/\beta} = 7.75\%$ is the effective (Mg + Zn) wt pct in Al 7075 sheet, while $C_{T_2}^{\mathrm{liq}/\alpha} = 30\%$ is extrapolated from the pseudo-binary Al-$MgZn_2$ phase diagram.[58]

A wide range of high-temperature diffusion coefficient values have been published for both Mg and Zn in binary aluminum alloys.[12] Since the diffusion coefficients of Mg

and Zn lie within the same scatter band, the choice of zinc as the rate-controlling element in the dissolution process is not unreasonable.[13] The dissolution time for liquid drops therefore is calculated using a D_{Zn} value of 0.1229×10^{-12} $m^2\ s^{-1}$ at 475 °C. The time t required for complete dissolution is determined from the relation

$$t = \left(\frac{R_0}{a}\right)^2$$

and is 0.06 to 1.4 seconds for a liquid drop having a radius R_0 of 100 to 500 nm. When the dissolution of platelike drops in a semi-infinite matrix is considered, the particle thickness varies with time according to the relation

$$B = B_0 - \frac{k}{\sqrt{\pi}}\sqrt{Dt}$$

where B is the particle thickness, B_0 is the initial thickness, and $k = a^2/D$. The time for complete dissolution is 0.12 to 3.0 seconds, assuming an initial thickness of 100 to 500 nm using the same diffusion coefficient for zinc. A calculated dissolution time of 0.06 seconds suggests that liquid drops might dissolve almost immediately following initiation of the dwell period. However, it is important to point out that the dimensions of the stir zone formed during spot welding significantly increase during the dwell period when material from the location beneath the tool shoulder moves downward and mixes with the lower sheet material.[59] As a result, upper and lower sheet materials continue to be incorporated into the stir zone as the dwell period progresses.

ACKNOWLEDGMENT

The authors acknowledge the financial support from the Natural Sciences and Engineering Research Council of Canada during this project.

REFERENCES

1. W.M. Thomas, E.D. Nicholas, J.D. Needham, M.G. Murch, P. Templesmith, and C.J. Daws: G.B. Patent Application No. 9,125,978.8, Dec. 1991; U.S. Patent No. 5,460,317, Oct. 1995.
2. C.G. Rhodes, M.W. Mahoney, and W.H. Bingel: *Scripta Mater.*, 1997, vol. 36, pp. 69-75.
3. T. Shibayanagi and M. Maeda: *Trans. JWRI*, 2004, vol. 33, pp. 17-23.
4. R.S. Mishra and M.W. Mahoney: *Mater. Sci. Forum*, 2001, vol. 357-359, pp. 507-14.
5. J.-Q. Su, T.W. Nelson, M. Mishra, and M. Mahoney: *Acta Mater.*, 2003, vol. 51, pp. 713-29.
6. J.-Q. Su, T.W. Nelson, and C.J. Sterling: *Scripta Mater.*, 2005, vol. 52, pp. 135-40.
7. M.L. Santella, T. Pan, T. Engstrom, and D. Storjohann: *SAE Technical Series*, SAE, Warrendale, PA, 2005, 2005-01-1249.
8. K. Nakata, S. Inoki, Y. Nagano, T. Hashimoto, S. Johgan, and M. Ushio: *J. Jpn. Inst. Light Met.*, 2001, vol. 51, pp. 528-33.
9. P.-C. Lin, S.-H. Lin, J. Pan, T. Pan, J.M. Nicholson, and M.A. Garman: *SAE Technical Series*, SAE, Warrendale, PA, 2004, 2004-01-1330.
10. P. Su, A. Gerlich, T.H. North, and G.J. Bendzsak: *SAE Technical Series*, SAE, Warrendale, PA, 2006, 2006-01-0971.
11. Ø. Frigaard, Ø. Grong, J. Hjelen, S. Gulbrandsen-Dahl, and O.T. Midling: *Proc. 1st Int. Symp. on Friction Stir Welding*, Thousand Oaks, CA, 1999, TWI, Great Abington, Cambridge, U.K., 1999.
12. P.-E. Droenen and N. Ryum: *Metall. Trans. A*, 1994, vol. 25A, pp. 521-30.
13. B. Bjørneklett, Ø. Frigaard, Ø. Grong, O.R. Myhr, and O.T. Midling: *Proc. 6th Int. Conf. on Aluminium Alloys*, Toyoashi, Japan, 1998, Japan Institute of Light Metals, Tokyo, Japan, 1988, pp. 1531-36.
14. J.R. Davis: *Aluminum and Aluminum Alloys*, ASM INTERNATIONAL, Materials Park, OH, 1993, p. 699.
15. H.J. McQueen and J.J. Jonas: *Treatise on Materials Science Technology*, Academic Press, New York, NY, 1975, vol. 6, pp. 393-493.
16. H.J. McQueen and J.E. Hocket: *Metall. Trans. A*, 1970, vol. 1, pp. 2997-3004.
17. G. Avramovic-Cingara, H.J. McQueen, A. Hopkins, V. Jain, and D. Perovic: in *Light Weight Alloys for Aerospace Applications*, E.W. Lee, N.J. Kim, and K.V. Jata, eds., Las Vegas, NV, TMS-AIME, Warrendale, PA, pp. 333-47.
18. G. Avramovic-Cingara and H.J. McQueen: *Aluminium,* 1994, vol. 70 (3–4), pp. 214-19.
19. G. Avramovic-Cingara, D.D. Perovic, and H.J. McQueen: *Metall. Mater. Trans. A*, 1996, vol. 27A, pp. 3478-90.
20. E. Cerri, E. Evangelista, A. Forcellese, and H.J. McQueen: *Mater. Sci. Eng.*, 1995, vol. A197, pp. 181-98.
21. T. Sheppard: *2nd Int. Conf. on Aluminum Alloys—Their Physical and Mechanical Properties,* C.Q. Chen and E.A. Starke, eds., International Academic Publisher, Beijing, pp. 744-54.
22. K.A.A. Hassan, B.P. Wynne, and P.B. Prangnell: *Proc. 4th Int. Conf. Friction Stir Welding*, Park City, UT, 2003, TWI, Great Abington, Cambridge, U.K.
23. P.N. Adler and R. Delasi: *Metall. Trans. A*, 1977, vol. 8A, pp. 1185-90.
24. Y.S. Sato, M. Urata, and H. Kokawa: *Metall. Mater. Trans. A*, 2002, vol. 33A, pp. 625-35.
25. C.I. Chang, C.J. Lee, and J.C. Huang: *Scripta Mater.*, 2004, vol. 51, pp. 509-14.
26. C.G. Rhodes, M.W. Mahoney, W.H. Bingel, and M. Calabrese: *Scripta Mater.*, 2003, vol. 48, pp. 1451-55.
27. K. Nakata, S. Inoki, Y. Nagano, T. Hashimoto, S. Johgan, and M. Ushio: *Proc. 3rd Int. Conf. Friction Stir Welding*, Kobe, Japan, 2001, TWI, Great Abington, Cambridge, U.K.
28. A. Gerlich, G.A. Cingara, and T.H. North: in *Aluminum Alloys 2006*, W.J. Poole, M.A. Wells, and D.J. Lloyd, eds., 2006, Materials Science Forum, vol. 519-521, pp. 1107-12.
29. F.J. Humphreys: *J. Mater. Sci.*, 2001, vol. 36, pp. 3833-54.
30. M. Karlsen, S. Tangen, J. Hjelen, Ø. Frigaard, and Ø. Grong: *Proc. 3rd Int. Conf. Friction Stir Welding*, Kobe, Japan, 2001, TWI, Great Abington, Cambridge, U.K.
31. M.W. Mahoney, C.G. Rhodes, J.G. Flintoff, R.A. Spurling, and W.H. Bingel: *Metall. Mater. Trans. A*, 1998, vol. 29A, pp. 1955-64.
32. F.J. Frost and M.F. Ashby: *Deformation-Mechanism Maps*, Pergamon Press, New York, NY, 1982.
33. K.V. Jata and S.L. Semiatin: *Scripta Mater.*, 2000, vol. 43 (8), pp. 743-49.
34. D. Schmitter and I.M. Zylla: *J. Phys. IV France*, 2004, vol. 120, pp. 677-80.
35. G.J. Bendzsak, T.H. North, and C.B. Smith: *Proc. 2nd Int. Conf. Friction Stir Welding*, Gothenburg, Sweden, 2000, TWI, Great Abington, Cambridge, U.K.
36. F.P. Bowden and K.E.W. Ridler: *Proc. R. Soc. London, Ser. A*, 1936, vol. 154 (883), pp. 640-56.
37. F.P. Bowden and P.H. Thomas: *Proc. R. Soc. London, Ser. A*, 1954, vol. 223 (1152), pp. 29-40.
38. A. Gerlich, P. Su, G.J. Bendzsak, and T.H. North: in *Friction Stir Welding and Processing III,* K.V. Jata, M.W. Mahoney, and R.S. Mishra, eds., TMS, Warrendale, PA, 2005.
39. T.F.J. Quinn and W.O. Winer: *Wear*, 1985, vol. 102, pp. 67-80.
40. T.H. North, G.J. Bendzsak, C.B. Smith, and G.H. Luan: *Proc. 7th Int. Symp. JWS*, Kobe, Japan, 2001, JWS, Tokyo, Japan, pp. 621-32.
41. T.H. North, G.J. Bendzsak, and C.B. Smith: *Proc. 2nd Int. Conf. Friction Stir Welding*, Gothenburg, Sweden, 2000, TWI, Great Abington, Cambridge, U.K.
42. A. Gerlich, P. Su, and T.H. North: *Sci. Technol. Welding Joining*, 2005, vol. 10, pp. 647-52.
43. A. Gerlich, P. Su, T.H. North, and G.J. Bendzsak: *Mater. Forum*, 2005, vol. 29, pp. 290-94.
44. A. Gerlich, P. Su, and T.H. North: *J. Mater. Sci.*, 2005, vol. 40, pp. 6473-81.
45. Kh.A.A. Hassan, P.B. Prangnell, A.F. Norman, D.A. Price, and S.W. Williams: *Sci. Tech. Welding Joining*, 2003, vol. 8, pp. 257-68.

46. Y. Yan, B. Lui, and C. Zhang: *Proc. 6th Int. Conf. on Aluminium Alloys*, Toyoashi, Japan, 1998, Japan Institute of Light Metals, Tokyo, Japan, 1988, pp. 1135-40.
47. C. Dalle-Donne, B. Braun, G. Staniek, A. Jung, and W.A. Kayser: *Materialwiss. Werkstofftech.*, 1998, vol. 29, pp. 609-17.
48. A. Gerlich, P. Su, and T.H. North: in *Magnesium Technology 2005*, N.R. Neelameggham, H.I. Kaplan, and B.R. Powell, eds., TMS, Warrendale, PA, 2005, pp. 383-88.
49. Y.S. Sato, S. Hwan, C. Park, M. Michiuchi, and H. Kokawa: *Scripta Mater.*, 2004, vol. 50 (9), pp. 1233-36.
50. P.A. Colegrove, H.R. Shercliff, and P.L. Threadgill: *Proc. 4th Int. Conf. Friction Stir Welding*, Park City, UT, 2003, TWI, Great Abington, Cambridge, U.K.
51. O. Reiso, H.-G. Øverlie, and N. Ryum: *Metall. Trans.*, 1990, vol. 21A, pp. 1689-95.
52. S. Kou: *Welding Metallurgy,* 2nd ed., Wiley & Sons, New York, NY, 2003, pp. 303-39.
53. W.F. Savage, E.F. Nippes, and J.D. Varsik: *Welding J.*, 1979, vol. 58, pp. 45s-52s.
54. X.-M. Li and M.J. Starink: *Mater. Sci. Technol.*, 2001, vol. 17, pp. 1324-28.
55. O.R. Myhr and Ø. Grong: *Acta Metall. Mater.*, 1991, vol. 39, pp. 2693-702.
56. M.J. Whelan: *Met. Sci. J.*, 1969, vol. 3, pp. 95-97.
57. P. Su, A. Gerlich, M. Yamamoto, and T.H. North: *Proc. Magnesium Technology in the Global Age Symp.*, 2006, CIM, Montreal, Canada.
58. H. Hanemann and A. Schrader: *Ternäre Legierungen des Aluminiums*, Verlag Stahleisen M.B.H., Dusseldorf, 1952, p. 138.
59. P. Su, A. Gerlich, T.H. North, and G.J. Bendzsak: *Sci. Technol. Welding Joining*, 2006, vol. 11, pp. 61-71.